The Plant Cell, Vol. 32: 2964–2978, September 2020, www.plantcell.org © 2020 ASPB.

LUNAPARK Is an E3 Ligase That Mediates Degradation of ROOT HAIR DEFECTIVE3 to Maintain a Tubular ER Network in Arabidopsis

Jiaqi Sun, Nooshin Movahed, and Huanquan Zheng[1]

Department of Biology, McGill University, Montreal, Quebec H3A 1B1, Canada

ORCID IDs: 0000-0003-4359-9896 (J.S.); 0000-0001-8852-245X (N.M.); 0000-0003-2986-725X (H.Z.)

ROOT HAIR DEFECTIVE3 (RHD3) is an atlastin GTPase involved in homotypic fusion of endoplasmic reticulum (ER) tubules in the formation of the interconnected ER network. Because excessive fusion of ER tubules will lead to the formation of sheet-like ER, the action of atlastin GTPases must be tightly regulated. We show here that RHD3 physically interacts with two Arabidopsis (*Arabidopsis thaliana*) LUNAPARK proteins, LNP1 and LNP2, at three-way junctions of the ER, the sites where different ER tubules fuse. Recruited by RHD3 to newly formed three-way junctions, LNPs act negatively with RHD3 to stabilize the nascent three-way junctions of the ER. Without this LNP-mediated stabilization, in Arabidopsis *lnp1-1 lnp2-1* mutant cells, the ER becomes a dense tubular network. Interestingly, in *lnp1-1 lnp2-1* mutant cells, the expression level of RHD3 is higher than that in wild-type plants. RHD3 is degraded more slowly in the absence of LNPs as well as in the presence of MG132 and concanamycin A. However, in the presence of LNPs, the degradation of RHD3 is promoted. We have provided in vitro evidence that Arabidopsis LNPs have E3 ubiquitin ligase activity and that LNP1 can directly ubiquitinate RHD3. Our data show that after ER fusion is completed, RHD3 is degraded by LNPs so that nascent three-way junctions can be stabilized and a tubular ER network can be maintained.

INTRODUCTION

The endoplasmic reticulum (ER) is an interconnected network of membranous tubules and sheets that stretches throughout the cytoplasm of eukaryotic cells. The ER plays important roles in the biosynthesis and transport of proteins and lipids, and it is an important architectural scaffold that helps maintain an ordered distribution of other cellular organelles (English and Voeltz, 2013). The ER is also important for calcium signaling, general cellular homeostasis, and cell growth (Angelos et al., 2017). Live-cell imaging has revealed that the ER is constantly remodeling, with continuous fusion of tubules (Sparkes et al., 2011), to make an interconnected ER network. The remodeling is important for the ER to perform various functions such as maintaining an ordered distribution of other organelles during cell growth and responding to different environmental stimuli (Westrate et al., 2015). Recent work indicates that the fusion of ER tubules is mediated by a class of ER membrane-bound, dynamin-like large GTPases (Hu et al., 2009; Orso et al., 2009). Plants have a dynamin-like GTPase known as ROOT HAIR DEFECTIVE3 (RHD3; Chen et al., 2011), that acting as a dimer in ER membranes, is believed to attach to and tether two opposing ER membranes and then fuse them through a GTP hydrolysis–dependent conformational change (Sun and Zheng, 2018). Because excessive fusion of the ER mediated by RHD3 leads to an abnormal sheet-like ER (Zheng and Chen, 2011), the action of RHD3 must be tightly regulated.

Recently, in yeast and mammalian cells, a family of proteins called LUNAPARK (LNP) has been reported to stabilize the formation of the tubular ER (Chen et al., 2015, 2018). It is proposed that LNP antagonizes the action of Sey1p and atlastin, the yeast and mammalian homologs of RHD3, respectively (Chen et al., 2012b). However, how LNP antagonizes Sey1p or atlastin is not clear and is, in fact, very controversial. Yeast Lnp1p has been found to physically interact with Sey1p (Chen et al., 2012b), while mammalian mLnp1 does not physically interact with atlastin (Wang et al., 2016). When the soluble domain of mammalian mLnp1 is purified, there is no significant effect on the fusion activity of atlastin in vitro (Chen et al., 2015). Also, mLnp1 purified from mammalian cells has a ubiquitin ligase activity, yet its substrate(s) has not been reported (Zhao et al., 2016). Plant homologs of LNP have been reported (Kriechbaumer et al., 2018; Ueda et al., 2018). Based on the increased mesh size of the tubular ER network in developed epidermal cells of hypocotyls and cotyledons of *lnp* mutants, it was suggested that plant LNP proteins are not functional homologs of yeast or mammalian Lnp1 and do not play a role in the formation of the tubular ER, but in the formation of the cisternal ER (Kriechbaumer et al., 2018; Ueda et al., 2018).

Here, we report that RHD3 interacts with two Arabidopsis (*Arabidopsis thaliana*) LNPs, LNP1 and LNP2. Arabidopsis *lnp1-1 lnp2-1* mutants have short root hairs and pleiotropic developmental growth defects including an abnormal ER with dense three-way junctions. We show that LNPs can be recruited by RHD3 to three-way junctions of the ER and are required for stabilizing newly formed three-way junctions of the ER. Our molecular evidence indicates that LNPs suppress the action of RHD3. In *lnp1-1 lnp2-1* mutants the expression level of RHD3 is higher than

[1] Address correspondence to hugo.zheng@mcgill.ca.
The author responsible for distribution of materials integral to the findings presented in this article in accordance with the policy described in the Instructions for Authors (www.plantcell.org) is: Huanquan Zheng (hugo.zheng@mcgill.ca).
www.plantcell.org/cgi/doi/10.1105/tpc.18.00937

IN A NUTSHELL

Background: Plant cells have numerous membrane-bound compartments in which many biological reactions critical for proper cell development and function occur. The endoplasmic reticulum (ER) is a compartment that is organized into a netlike labyrinth of interconnected tubules and flattened sheets in which proteins and lipids are synthesized and processed. The formation and maintenance of this labyrinth-like structure requires fusion of different ER tubules. These fusion events are mediated by ROOT HAIR DEFECTIVE3 (RHD3). Because uncontrolled action of RHD3 would lead to excessive fusion, the action of RHD3 must be tightly regulated. Otherwise, abnormal ER will be formed in cells, leading to improper cell development and defective responses to stresses.

Questions: Is the action of RHD3 regulated by other factors, and if so, how is the activity of RHD3 regulated?

Findings: We first found that RHD3 physically interacts with two proteins called LUNAPARK1 (LNP1) and LUNAPARK2 (LNP2) in Arabidopsis. After the fusion of different ER tubules is completed, RHD3 recruits either LNP1 or LNP2 to a so-called 3-way junction site of the ER where different ER tubules fuse. Subsequently, RHD3 disappears from the site. In this way, a newly formed 3-way junction site becomes stable. How do LNPs make RHD3 disappear? We found that both LNP1 and LNP2 can act as E3 ligases to ubiquitinate RHD3, which is then degraded. In Arabidopsis *lnp1 lnp2* double mutant cells, RHD3 can not be degraded efficiently, leading to unstable newly formed 3-way junctions and sheet-like ER.

Next steps: LNPs form an evolutionarily conserved family of proteins, but there is no typical E3 domain in LNPs. Our next questions to answer are: 1) how do LNPs function as E3 ligases?; 2) do LNPs act on other ER-shaping proteins?; and 3) are LNPs involved in ER autophagy so to maintain ER homeostasis?

that in wild-type plants. Both our in vitro and in vivo data suggest that LNPs promote the degradation of RHD3 through ubiquitination. We further revealed that Arabidopsis LNPs have an E3 ubiquitin ligase activity and that LNP1 can directly ubiquitinate RHD3 in vitro. Thus, we concluded that there is an LNP-mediated RHD3 protein degradation following the formation of three-way junctions of the ER so that the newly formed three-way junctions of the ER can be stabilized.

RESULTS

RHD3 Physically Interacts with LNPs in Plants

To better understand how the action of RHD3 is regulated, as well to dissect the detailed mechanisms by which the tubular ER network is maintained, we developed a 3-in-1 bimolecular fluorescence complementation (BiFC)–based screening system in *Nicotiana benthamiana* (Supplemental Figure 1A) to identify potential interacting proteins of RHD3. In this system, there are three independent open reading frames (ORFs) in the construct. One ORF encodes the ER lumen marker mCherry-HDEL, which serves as an internal reference for protein expression and also as an ER marker for the localization of possible interactions. Another ORF contains RHD3 fused with the N-terminal domain of Venus, as RHD3 with a C-terminal fusion is not functional (Chen et al., 2011). Potential RHD3-interacting proteins were fused to the C-terminal domain of Venus in the third ORF. We chose 15 proteins that are predicted to be ER localized and may have a role in maintaining ER morphology as the candidates. Using this system, we identified two proteins, LNP1 (AT2G24330) and LNP2 (AT4G31080; Kriechbaumer et al., 2018) that interacted with RHD3 (Figures 1A to 1E). Both LNPs shared a conserved N terminus, two transmembrane domains, a coiled-coil domain, and one C terminus containing a zinc finger motif, similar to LNP proteins found in yeast and mammalian cells (Supplemental Figures 1B and 1C). A phylogenetic analysis (Supplemental Figure 2) of homologs of LNPs indicated that LNPs formed a family of proteins that were evolutionarily conserved across eukaryotic species.

Interestingly, in our BiFC assay both LNPs interacted with RHD3 on three-way junctions of the ER, indicated by mCherry-HDEL (Figures 1A and 1B, enlargements). RHD3 did not interact with the negative control p24 (Figure 1C), an ER membrane protein involved in the transport between ER and Golgi (Chen et al., 2012a). Also, LNP1 or LNP2 did not interact with CER6 (Figures 1D and 1E), an ER-localized, very long fatty acid–condensing enzyme that catalyzes the elongation of C22 fatty acyl-CoAs or longer (Hooker et al., 2002).

To verify the interaction between RHD3 and LNP proteins, we used the mating-based split-ubiquitin system (SUS; Grefen et al., 2007), and we found that both LNP1 and LNP2 interacted with RHD3 in yeast cells (Figure 1F, rows 3 and 4). Consistent with the previous results (Chen et al., 2011; Sun and Zheng, 2018), RHD3 interacted with itself (Figure 1F, row 1, served as the positive control), but not with NubG alone (Figure 1F, row 2, served as the negative control). A GFP-trap beads–based pull-down assay was also conducted in *lnp1-1* plants expressing pLNP1pro:LNP1-YFP with mCherry-HDEL or mCherry-RHD3. As indicated in Figure 1G, mCherry-RHD3, but not mCherry-HDEL, was pulled down together with LNP1-YFP by GFP-trap beads. Similarly, when coexpressed in *N. benthamiana*, mCherry-RHD3 could be copurified with LNP1-YFP or LNP2-YFP (Supplemental Figures 3A and 3B). Taken together, we conclude that RHD3 physically interacts with LNP1 and LNP2.

LNPs Are Required for Normal Cell Development and for Maintenance of Tubular ER Network

We first wondered whether LNP1 and LNP2 play any role in plant cell development. To study this, we identified two T-DNA

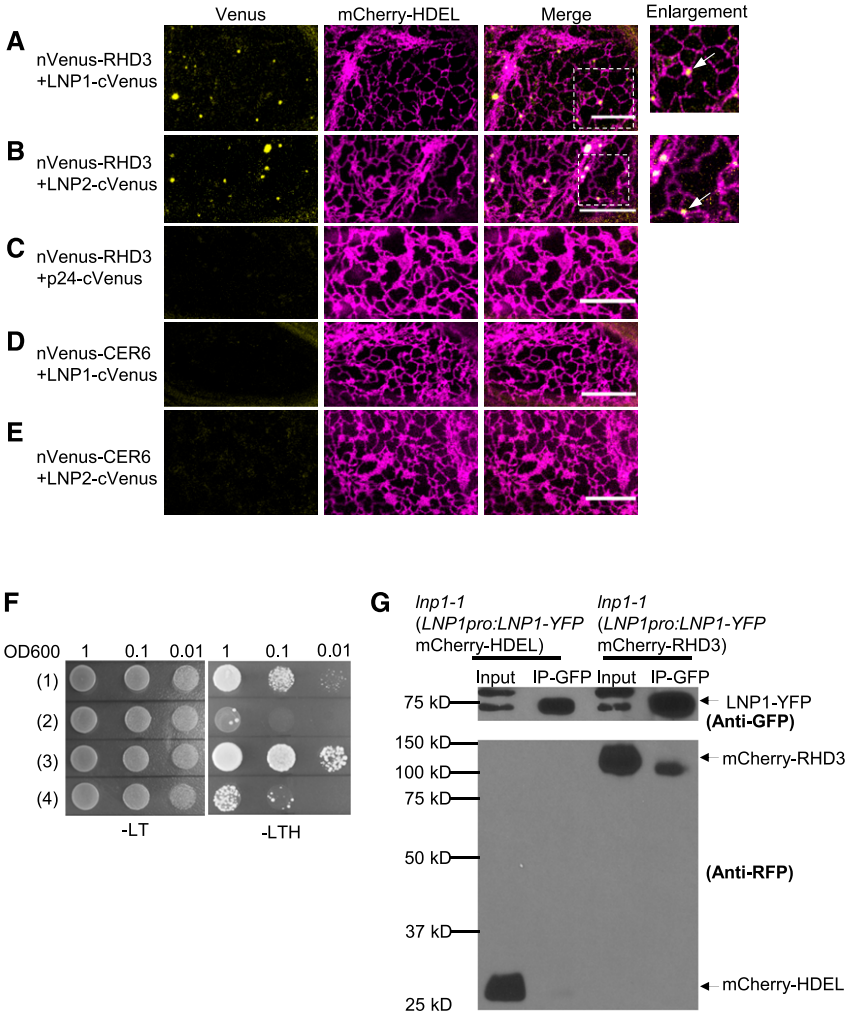

Figure 1. RHD3 Interacts with LNP Proteins.

(A) and **(B)** RHD3 interacts with LNP1 **(A)** and LNP2 **(B)** in three-way junctions (white arrows) of the ER in epidermal cells of *N. benthamiana* leaves. The white dashed boxes outline the enlarged areas to the right, and the white arrows point at the interaction on the three-way junctions. Bars = 10 μm.
(C) RHD3 does not interact with p24 (negative control). Bars = 10 μm.
(D) and **(E)** LNP1 **(D)** and LNP2 **(E)** do not interact with CER6 (negative control). Bars = 10 μm.
(F) Interactions identified using the mating-based split-ubiquitin system. (1) The positive control, Cub-RHD3+NubG-RHD3, shows an interaction. (2) The negative control, Cub-RHD3+NubG, shows that Cub-RHD3 does not interact with NubG. (3) Cub-RHD3+LNP2-NubG shows that Cub-RHD3 interacts with LNP2-NubG. (4) Cub-RHD3+LNP1-NubG shows that Cub-RHD3 interacts with LNP1-NubG. Mated diploid yeast cells were diluted into $OD_{600\,nm}$ = 1, 0.1, and 0.01 as indicated. The diploid cells were plated onto -LT SC medium to verify the mating and on -LTH SC medium to verify the interaction.
(G) Immunoblot of proteins immunoprecipitated (IP) with GFP-trap beads. *lnp1-1* plants expressing *LNP1pro:LNP1-YFP* with mCherry-HDEL or mCherry-RHD3 were used for IP. The predicted size of mCherry-RHD3 and LNP1-YFP is 117 and 78 kD, respectively.

insertional knockdown *lnp1* mutant alleles, *lnp1-1* (GK607D07) and *lnp1-2* (SK2564), and two T-DNA insertional knockout *lnp2* mutant alleles, *lnp2-1* (SALK_028863) and *lnp2-2* (SALK_100743; Figures 2A and 2B). Compared with wild-type seedlings, single *lnp1-1* and *lnp2-1* mutants had slightly shorter root hairs and double mutant *lnp1-1 lnp2-1* had significantly shorter root hairs (Figure 2D). In terms of general plant cell and tissue development, a single *lnp1-1* or *lnp2-1* mutant did not appear to have any obvious defects, but the cotyledons and leaves of double mutant plants were much smaller than those of the wild-type plants (Figure 2C). The defects in root hairs and other tissues of the double mutant *lnp1-1 lnp2-1* could be rescued by the transformation with either LNP1-YFP or LNP2-YFP alone driven by their native promoters (Figures 2C and 2D). These results suggested that the yellow fluorescent protein (YFP)–tagged LNP1 and LNP2 fusion proteins are fully functional in vivo and that it is likely that LNP1 and LNP2 have redundant functions in plant cell development in Arabidopsis.

In *rhd3* mutants, the ER is bundled and less branched, so we investigated whether *lnp* mutants are also defective in ER

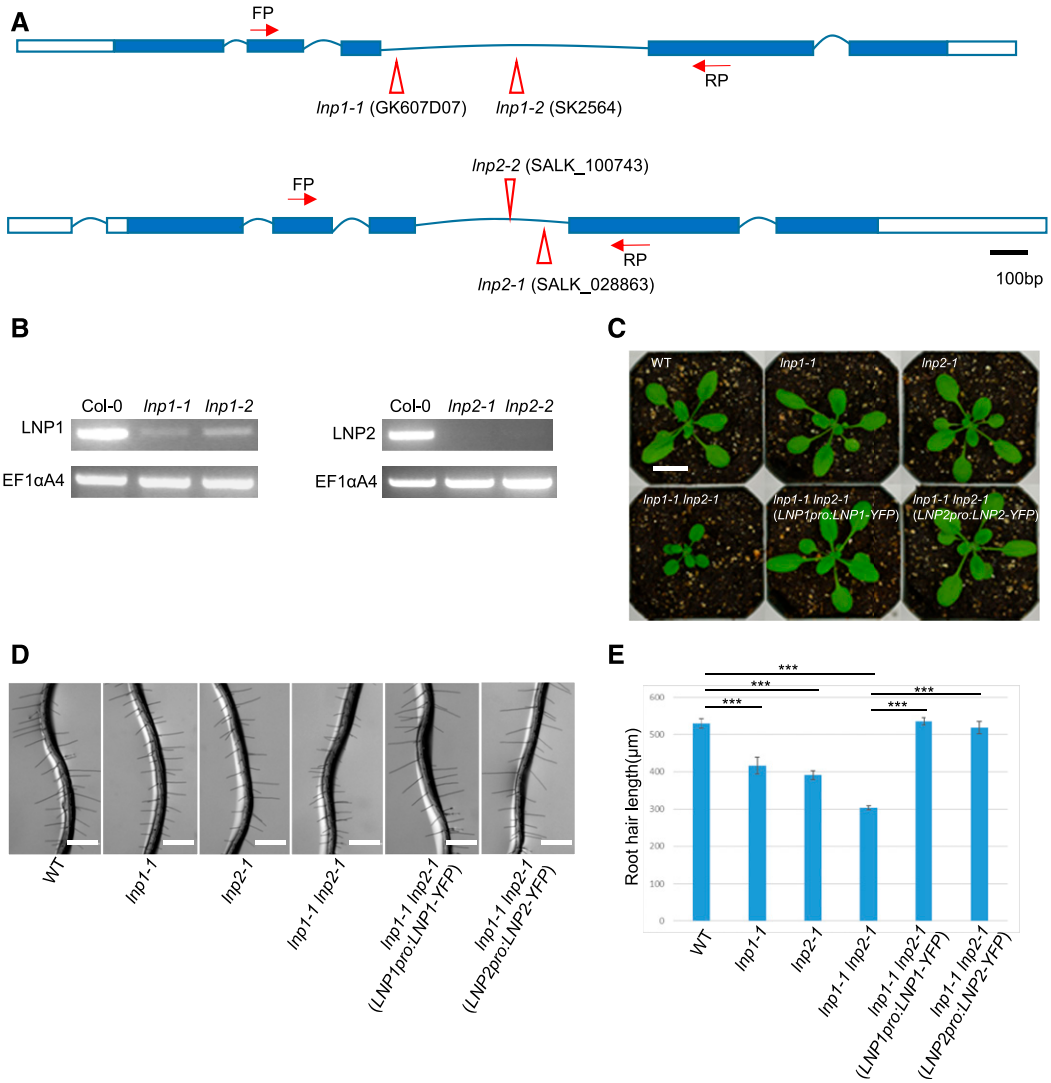

Figure 2. *LNP*s Are Required for Normal Plant Cell Development.

(A) *LNP1* and *LNP2* structures. The white boxes indicate untranslated regions, the blue boxes indicate exons, and the curved lines indicate the introns. The triangles indicate T-DNA insertion positions in the *lnp1* and *lnp2* lines. FP and RP are the primers used for RT-PCR.
(B) RT-PCR analysis of different *lnp1* (left) and *lnp2* (right) T-DNA mutants. EF1αA4 was used as the loading control.
(C) Developmental defects of *lnp1-1 lnp2-1* mutants and molecular complementation of *lnp1-1 lnp2-1*. The double mutant was complemented with either *LNP1-YFP* or *LNP2-YFP*, each driven by its native promoter ($LNP1_{pro}$ or $LNP2_{pro}$). Bar = 2 cm. WT, wild type.
(D) Root hair phenotypes of *lnp1* and *lnp2* mutants and molecular complementation of *lnp1-1 lnp2-1*. Bars = 100 μm. WT, wild type.
(E) Quantification of root hair length in **(D)**. Data show means ± SE. Asterisks (***) indicate a significant difference from the wild type (WT; Student's *t* test, p-value < 0.001; Supplemental File 1). Ten seedlings (10 root hairs per seedling) were used for quantification.

morphology. YFP-HDEL was expressed in both wild-type Columbia-0 (Col-0) and *lnp1-1 lnp2-1* double mutants. Three days after germination, in the wild-type cotyledon cells, the ER was viewed as a tubular network (Figure 3A). However, in the double mutant *lnp1-1 lnp2-1* cotyledon cells, there were massive cortical ER sheets and large clumps of the cytoplasmic ER (Figure 3A, arrows) under conventional confocal microscopy. With Airyscan superresolution microscopy, we found that these cortical ER sheets were actually ER networks with dense junctions (Figure 3C, enlarged image), similar to what is described in mammalian cells (Nixon-Abell et al., 2016). In 5-d-old cotyledon cells of *lnp1-1 lnp2-1*, consistent with what was reported by Kriechbaumer et al. (2018) and Ueda et al. (2018), the mesh size of the cortical ER was increased (Figure 3B). However, there were also large clumps of the cytoplasmic ER (Figure 3B, arrows), which were not reported by Kriechbaumer et al. (2018) and Ueda et al. (2018). Using transmission electron microscopy, we found that the clumps of the cytoplasmic ER in *lnp1-1 lnp2-1* were in fact composed of dense ER tubules (Figure 3E, red asterisks). Such clumps were not observed in the wild type (Figure 3D). Taken

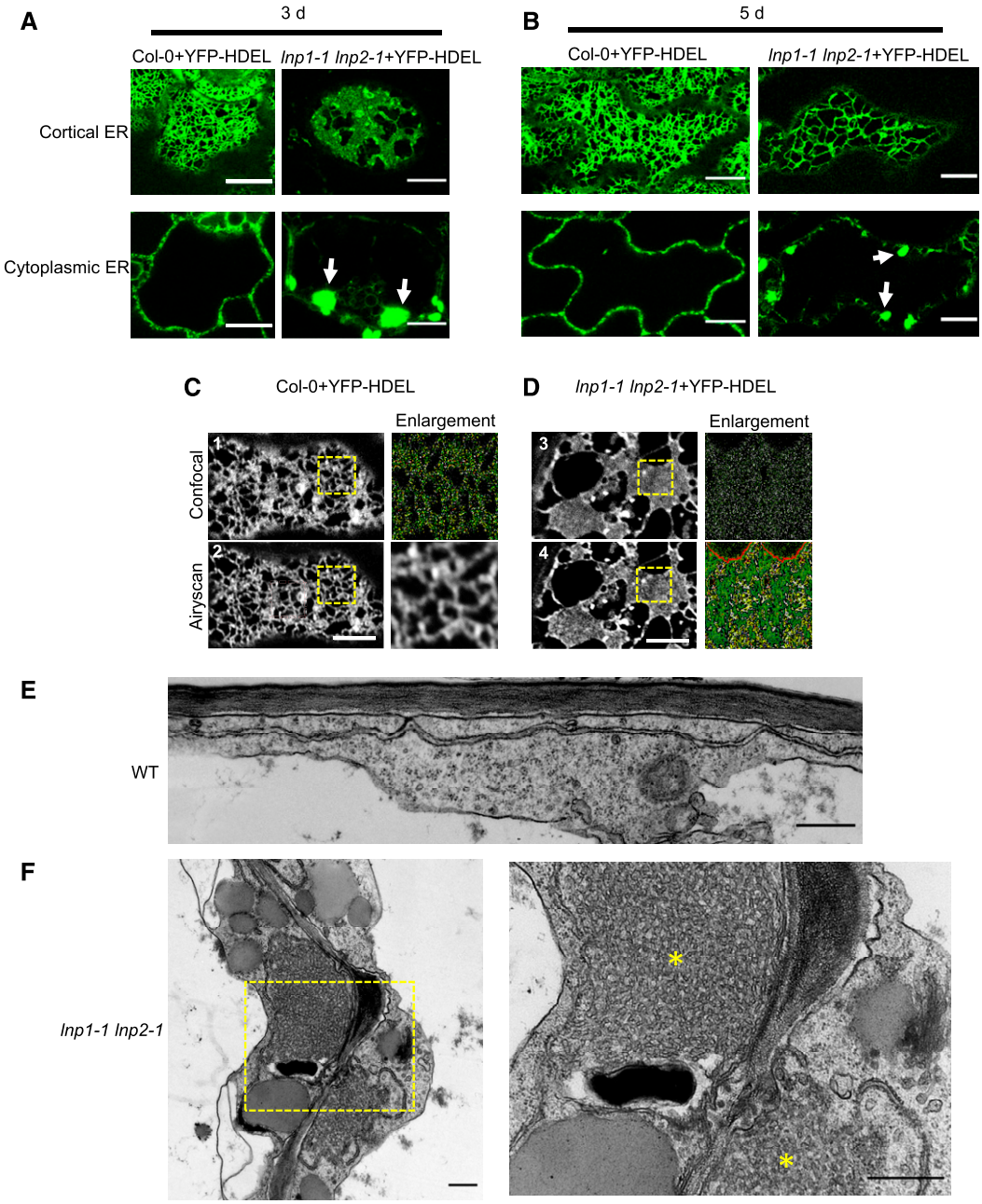

Figure 3. There Are More ER Sheets with Intensive Three-Way Junctions in *lnp1lnp2* Mutants.

(A) and **(B)** Cortical and cytoplasmic ER morphology of cotyledon epidermal cells of the 3-d-old **(A)** and 5-d-old **(B)** wild-type and *lnp1-1 lnp2-1* seedlings transformed with YFP-HDEL driven by the 35S promoter. Arrows indicate clumps of the ER. Bars = 10 μm.

(C) Cortical ER morphology in cotyledon epidermal cells of the 3-d-old seedlings of the wild type and *lnp1-1 lnp2-1* expressing YFP-HDEL driven by the cauliflower mosaic virus 35S promoter. Photographs show confocal (1, 3) and Airyscan (2, 4) imaging of the ER network in the wild type (1, 2) or *lnp1-1 lnp2-1* (3, 4) expressing YFP-HDEL driven by the 35S promoter. The enlarged regions are indicated by dashed yellow squares. Compared with the wild type, there are much more dense ER junctions in *lnp1-1 lnp2-1* mutant cells. Bars = 5 μm.

(D) and **(E)** The ER in cotyledon cells of the 3-d-old wild-type (WT; see **[D]**) and *lnp1-1 lnp2-1* **(E)** seedlings analyzed at the ultrastructural level. The right image in **(E)** is the enlarged image from the left image, which is indicated by the dashed yellow square. Asterisks (*) indicate the large aggregates of ER tubules. Bars = 500 nm.

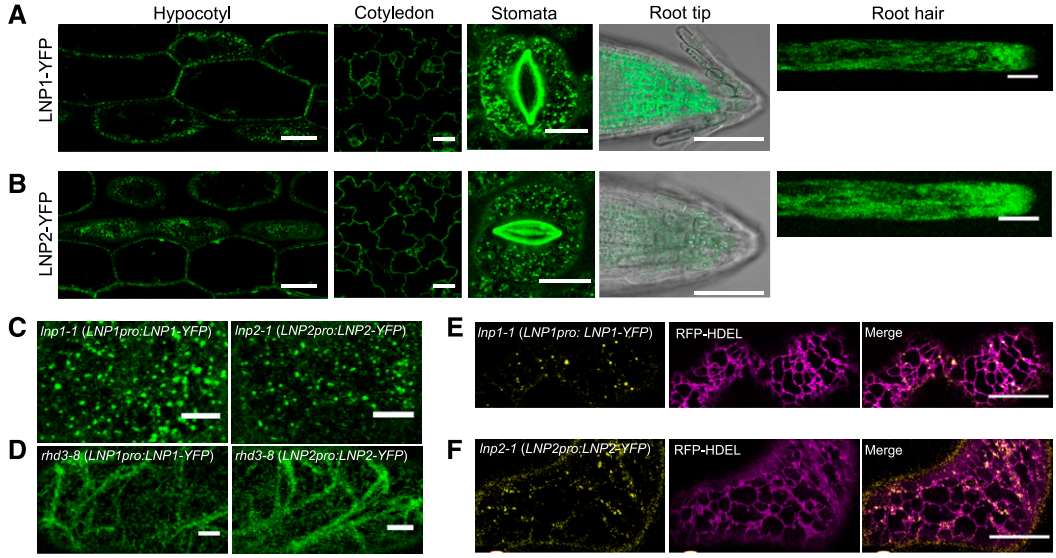

Figure 4. Expression and Subcellular Localization of LNP Proteins.

(A) and **(B)** Arabidopsis LNPs are expressed in young developing tissues. LNP1 **(A)** and LNP2 **(B)** are expressed in hypocotyl, cotyledon, stomata, root tips, and growing root hairs. Four days after germination, *lnp1-1*(*LNP1pro:LNP1-YFP*) and *lnp2-1*(*LNP2pro:LNP2-YFP*) seedlings were taken for imaging. Bars = 20 μm, except 5 μm in root hair images.

(C) Localization of LNP1 and LNP2 driven by their native promoters in the cortical region of a cotyledon epidermal cell. Both showed a punctate pattern. Bars = 5 μm.

(D) LNP1 and LNP2 are improperly localized to ER tubules in in the cortical region of cotyledon epidermal cells in *rhd3-8*. Bars = 5 μm.

(E) and **(F)** LNP1 **(E)** as well as LNP2 **(F)** is localized to three-way junctions of the ER. Images show cotyledon epidermal cells of *lnp1-1* or *lnp2-1* seedlings expressing LNP1-YFP or LNP2-YFP driven by its native promoter (left), RFP-HDEL driven by the cauliflower mosaic virus 35S promoter (center), and a merged image (right). Bars = 10 μm.

together, we conclude that Arabidopsis LNPs are involved in maintaining a normal tubular ER morphology.

LNPs Are Recruited by RHD3 to Three-Way Junctions of the ER Network

To understand how LNPs are required for maintaining a normal tubular ER morphology, we next examined their subcellular localization. To this end, we made LNP1-YFP and LNP2-YFP driven by their native promoters and then expressed them in *lnp1-1* and *lnp2-1* mutants. Expression of LNP1-YFP and LNP2-YFP overlapped in diverse highly developing tissues, including developing hypocotyl cells, young epidermal cells of cotyledons, stomatal cells, root tips, and growing root hairs (Figures 4A and 4B). This further suggested that LNP1 and LNP2 have redundant functions in different developing cell types. Detailed confocal microscopy of cotyledon epidermal cells indicated that LNP1-YFP and LNP2-YFP showed puncta localization (Figure 4C). These puncta were confirmed to be three-way junctions of the ER by expressing RFP-HDEL in *lnp1-1* (*LNP1pro*:*LNP1-YFP*) and *lnp2-1* (*LNP2pro*:*LNP2-YFP*) plants (Figures 4E and 4F). Strikingly, in the epidermal cells of the *rhd3-8* mutant, LNP1-YFP and LNP2-YFP were seen on ER tubules rather than in puncta (Figure 4D). When LNP1-RFP and LNP2-RFP were transiently overexpressed with OD = 0.1 in *N. benthamiana* leaves, LNP1-RFP and LNP2-RFP were observed in ER tubules in addition to their enrichment on three-way junctions of the ER (Supplemental Figures 4A and 4C), possibly due to the nature of transient overexpression (Sparkes et al., 2006). Interestingly, in the presence of YFP-RHD3, LNP1-RFP and LNP2-RFP were exclusively localized in three-way junctions of the ER, most of which were colocalized with YFP-RHD3 (Supplemental Figures 4B and 4D). However, in the presence of dominant-negative forms of RHD3(S51N) or RHD3(T75A) (Chen et al., 2011), the localization of LNP1-RFP (Supplemental Figures 4E and 4F) and LNP2-RFP (Supplemental Figures 4G and 4H) to the three-way junctions were lost; they were only localized on ER tubules. These results suggested that the localization of LNP1 and LNP2 to three-way junctions of the ER requires functional RHD3 and that LNP1 and LNP2 can be recruited by functional RHD3 to the three-way junctions of the ER.

LNP1 Stabilizes the Nascent Three-Way Junctions of the ER in Arabidopsis Cells

The ER with dense three-way junctions in *lnp1-1 lnp2-1* mutants and the localization of LNPs on three-way junctions of the ER in plant cells prompted us to examine what roles Arabidopsis LNPs may play in the formation of three-way junctions of the ER. To this end, we transiently coexpressed LNP1-RFP (OD = 0.01) with YFP-HDEL in *N. benthamiana* leaves. The dynamics of nascent three-way junctions of the ER within 200 s was then followed to quantify their existing time. We defined the starting time when a tubule fuses together with another tubule to form a three-way junction and the end time when the junctions disappear after the ring

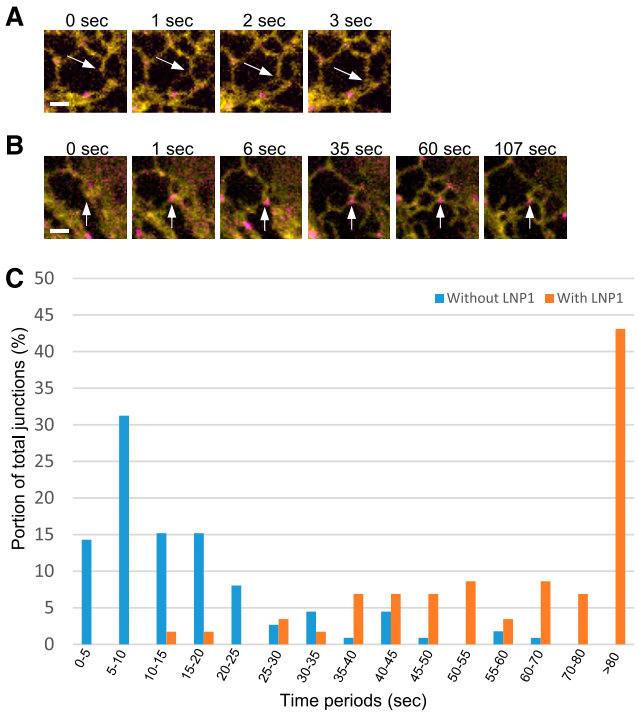

Figure 5. LNP1 Stabilizes Newly Formed Junctions of the ER.

(A) An example of an unstable newly formed ER junction lacking LNP1-RFP (white arrows). Without the presence of LNP1-RFP, the newly formed three-way junction (white arrows) disappears very quickly (<3 s) with a ring closure event. Bar = 1 μm.

(B) An example of a stable newly formed junction with LNP1-RFP (white arrows). The arrows point to the newly formed junction. YFP-HDEL and LNP1-RFP were coexpressed in the *N. benthamiana* leaves and observed 2 d after infiltration with OD = 0.01. Bar = 1 μm.

(C) Numbers of junctions with or without LNP1 present in different time periods were quantified. In total, 112 newly formed junctions without LNP1 and 58 newly formed junctions with LNP1 were observed.

closure. Of 170 newly formed three-way junctions examined, we found that 112 of them did not contain LNP1-RFP. Most of these junctions disappeared in 25 s (Figures 5A and 5C; Supplemental Movie 1), while of 58 of them with the presence of LNP1-RFP, many of these nascent junctions would exist more than 80 s (Figures 5B and 5C; Supplemental Movie 2). This result indicated that Arabidopsis LNPs stabilize the nascent three-way junctions of the ER in plant cells.

LNPs Suppress the Fusion Function of RHD3

Since LNPs interact with the RHD3 protein, we wondered whether LNPs stabilize nascent three-way junctions by regulating the fusion action of RHD3. It is known that, similar to the overexpression of atlastin (Nixon-Abell et al., 2016), overexpression of RHD3 leads to the formation of sheet-like ER (Zheng and Chen, 2011), which was indeed with dense junctions revealed by Airyscan superresolution microscopy (Supplemental Figure 5) as a result of excessive fusion of ER membranes. When YFP-HDEL was expressed alone in *N. benthamiana* leaves, only 10% of the cells had sheet-like ER (Figures 6A and 6E). We defined a sheet as an ER sheet when its area occupied several three-way junctions. When mCherry-RHD3 was coexpressed together with YFP-HDEL, sheet-like ER was found in more than 60% of the cells (Figures 6B and 6E). Intriguingly, for the coexpression of LNP1-YFP or LNP2-YFP with mCherry-RHD3, the percentage of cells with sheet-like ER was decreased to ~30% (Figures 6C to 6E). This implied that LNPs suppress the excessive fusion action of RHD3 that caused the formation of the sheet-like ER network.

To confirm that LNPs can suppress the fusion action of RHD3, we used a yeast ER fusion assay to quantify the ER fusion (Anwar et al., 2012). Consistent with previous studies by Zhang et al. (2013) and Sun and Zheng (2018), *Δsey1p* mutant cells exhibited slow ER fusion progress (~23 min; Figure 6F, column 1; Supplemental Movie 3), but the expression of RHD3 or Sey1p significantly improved the ER fusion efficiency (Figure 6F, columns 2 and 5; Supplemental Movies 4 and 5). However, coexpression of RHD3 with LNP1 or LNP2 together did not rescue the ER fusion defects in *Δsey1p* mutant (Figure 6F, columns 3 and 4; Supplemental Movies 6 and 7), suggesting that LNPs can suppress the fusion action of RHD3. It is interesting to note that neither Arabidopsis LNP1 nor LNP2 suppressed the fusion action of Sey1p when LNP1 or LNP2 was coexpressed with Sey1p in the *Δsey1p* yeast cells (Figure 6F, columns 5, 6, and 7; Supplemental Movies 8 and 9). Furthermore, we noted that Arabidopsis LNPs did not interact with Sey1p in our BiFC assay in *N. benthamiana* cells (Supplemental Figure 6). Thus, we believe that this LNPs-mediated suppression is specific to RHD3.

LNPs Promote the Protein Degradation of RHD3

Next, we wondered how LNPs could suppress the action of RHD3. We first found that in transient coexpression of YFP-RHD3 together with LNP1-RFP or LNP2-RFP in *N. benthamiana* (Figures 6C and 6D), the protein expression level of YFP-RHD3 was reduced compared to that when YFP-RHD3 was expressed alone (Supplemental Figure 7A). We then checked the expression level of RHD3 in the wild-type and *lnp1-1 lnp2-1* mutant plants with the anti-RHD3 antibody. The specificity of this anti-RHD3 antibody was confirmed by checking the expression of RHD3 in the *rhd3-8* mutant (Supplemental Figure 7B). More RHD3 accumulated both in young seedlings (Supplemental Figure 7B) and in older plants of *lnp1-1 lnp2-1* mutant than that in the wild-type plants (Figure 7A). There was no significant difference at the RNA level of *RHD3* (Figure 7B). The expression difference is much more obvious in the older plants (Figure 7A). Two additional ER proteins, AGB1 (Wang et al., 2007) and LPAT2 (Kim et al., 2005), were found to be similar between *lnp1-1 lnp2-1* and the wild-type plants (Figure 7A), suggesting there is no overall increase of the ER content in the absence of LNP1 and LNP2 (Figure 7A). These results indicated that LNPs may be involved in the degradation of RHD3 in plant cells.

A semi–in vitro cell-free protein degradation assay (Wang et al., 2009) was then used to compare the degradation rate of RHD3 between wild-type and *lnp1-1 lnp2-1* mutant plants. We found that in this semi–in vitro cell-free assay, RHD3 was degraded more slowly in the *lnp1-1 lnp2-1* mutant background than that in the wild type (Figure 7C). MG132, a drug that inhibits ubiquitin-dependent

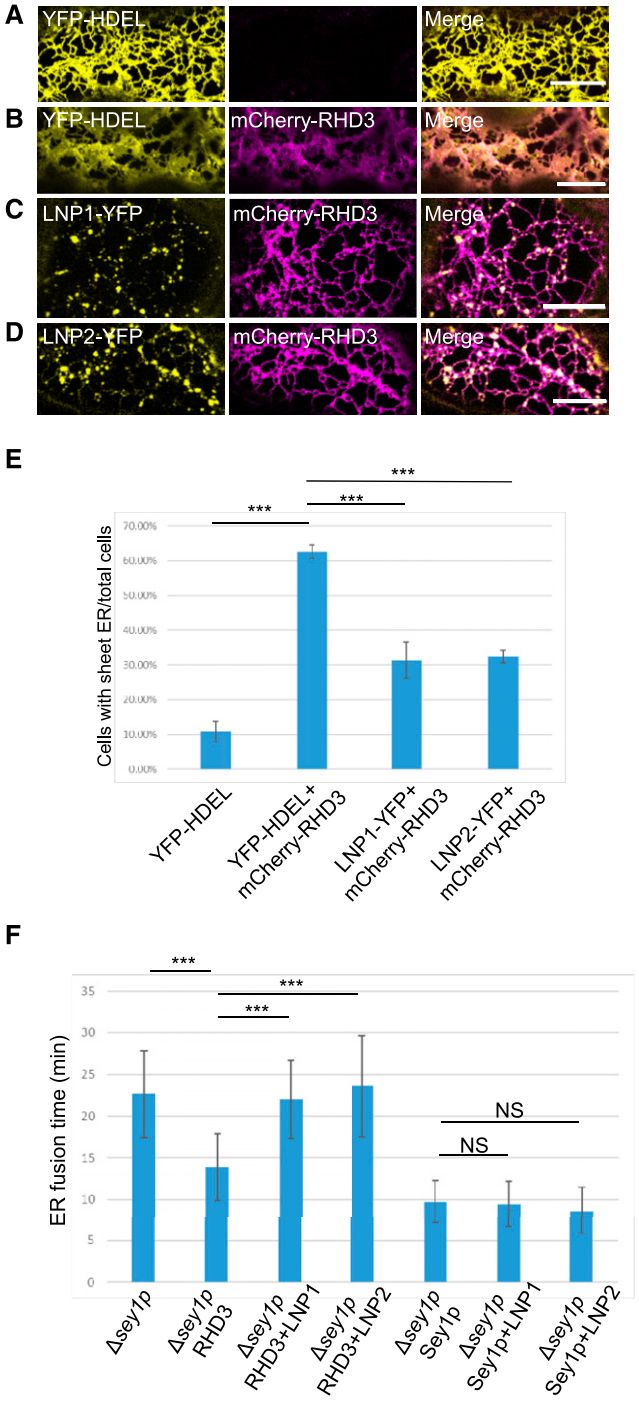

Figure 6. LNP Proteins Inhibit Fusion Action of RHD3.

(A) to **(D)** Representative images of four different transient expressions in epidermal cells of *N. benthamiana* leaves as indicated: **(A)** YFP-HDEL alone (OD = 0.01); **(B)** YFP-HDEL (OD = 0.01) and mCherry-RHD3 (OD = 0.1); **(C)** LNP1-YFP (OD = 0.01) and mCherry-RHD3 (OD = 0.1); and **(D)** LNP2-YFP (OD = 0.01) and mCherry-RHD3 (OD = 0.1). Bars = 10 μm.

(E) Quantification of the number of cells with sheet ER relative to the total cell number of cells examined in the four different infiltration conditions. Cells having more than 50% of their area covered by sheet-like ER were defined as cells with sheet ER. An ER is defined as an ER sheet when its area occupies several three-way junctions. At least 50 cells were examined for each condition. Data from three independent replicates show means ± SD. Asterisks (***) represent p-value < 0.001(Student's *t* test; Supplemental File 1).

(F) ER fusion efficiency test for different yeast strains indicated. Asterisks (***) represent p-value < 0.001(Student's *t* test; Supplemental File 1). Data show means ± SD of 20 to 50 fusion events that were used for quantification for each strain in three independent experiments. NS, no significant difference.

protein degradation by the 26S proteasome (Wang et al., 2009), also slowed the degradation of RHD3 (Figure 7C). Although a difference between the samples was detected in this cell-free protein degradation assay, the degradation of proteins was fast, as many factors are involved in protein degradation in this cell-free system (Wang et al., 2009). Therefore, we conducted an in vivo protein degradation assay after treatment with cycloheximide (CHX), a drug used to inhibit protein biosynthesis (Liu et al., 2015). Compared to that in the wild type, the degradation of RHD3 was much slower in *lnp1-1 lnp2-1* (Figure 7D), and MG132 also slowed the degradation of RHD3 (Figure 7D). We noted that MG132 did not fully inhibit the degradation of RHD3. Therefore, we tested whether concanamycin A (ConcA), a V-ATPase inhibitor that has been used to monitor autophagy-based protein degradation in plant cells (Yoshimoto et al., 2004). As indicated in Figure 7E, ConcA also partially inhibited the degradation of RHD3. When MG132 and ConcA were combined, the inhibition was comparable to that in *lnp1 lnp2* mutant cells (Figure 7E).

Furthermore, with dual fluorescent protein labeling, we found a gradual accumulation of mCherry-RHD3 at the newly formed three-way junctions (Supplemental Figure 8A, 0-5S) and the recruitment of LNP1-YFP to the junction (Supplemental Figure 8A, 4S), after which mCherry-RHD3 gradually disappeared (Supplemental Figure 8A, 5-18S). On the other hand, RHD3 puncta tended to accumulate over time in the absence of LNP1-YFP (Supplemental Figure 8B). In our observation, 35 out of 46 (76.1%) of RHD3 puncta were found to disappear in the presence of LNP1. However, in the absence of LNP1, the majority (30 out of 39; 76.9%) of the RHD3 puncta tended to accumulate, although some (9 out of 39; 23.1%) of the RHD3 puncta were found to disappear, possibly owning to the existence of the endogenous *Nicotiana tabacum* LNPs. Taken together, we conclude that LNPs promote the degradation of RHD3 in plant cells.

LNPs Are Involved in Ubiquitination of RHD3

Next, we wanted to understand how LNPs promoted the degradation of RHD3. We first checked whether RHD3 is ubiquitinated and whether this ubiquitination is changed in the absence of LNP1 and LNP2. We created *rhd3-8 lnp1-1 lnp2-1* (*RHD3pro*:*YFP-RHD3*) plants by crossing. YFP-RHD3 was then purified from *rhd3-8* (*RHD3pro*:*YFP-RHD3*) and *rhd3-8 lnp1-1 lnp2-1* (*RHD3pro*:*YFP-RHD3*) plants. When the same amount of purified YFP-RHD3 was loaded and blotted with the anti-ubiquitin antibody, YFP-RHD3 was indeed ubiquitinated and the ubiquitination level of YFP-RHD3 in *rhd3-8 lnp1-1 lnp2-1* (*RHD3pro*:*YFP-*

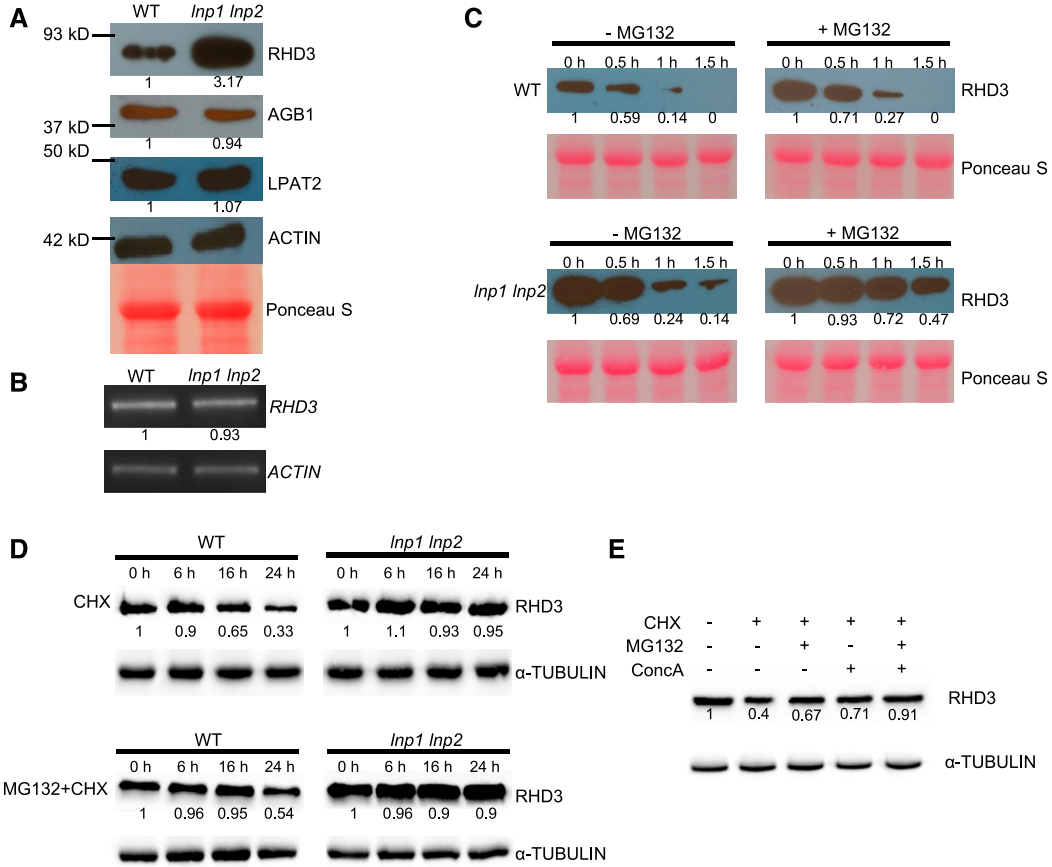

Figure 7. LNP Proteins Promote the Degradation of RHD3.

(A) Accumulation of RHD3 was elevated in *lnp1-1 lnp2-1* mutant plants. Ponceau S staining and actin were used as the loading controls. AGB1 and LPAT2 were used as ER reference proteins. Total proteins were extracted from the leaves of 4-week-old plants. The intensity of each band relative to the actin band was quantified and is indicated underneath the blot. Three independent experiments were performed with similar results. WT, wild type.

(B) RT-PCR of *RHD3* from the wild-type (WT) and *lnp1-1 lnp2-1* plants. The intensity of each band relative to the *ACTIN* band is quantified by ImageJ. Four independent experiments were performed with similar results.

(C) RHD3 is degraded slower in the *lnp1-1 lnp2-1* mutant background and in the presence of MG132 in the semi–in vitro degradation assay. Total proteins were extracted from the wild-type (WT) and *lnp1-1 lnp2-1* mutant plants with (+MG132) or without MG132 (–MG132). Band intensities were quantified relative to the protein amount at 0 h and are indicated underneath the blot. Ponceau S staining was used as a loading control. Three independent experiments were performed with similar results.

(D) In vivo degradation of RHD3. Seven-day-old seedlings were treated with 200 mM CHX (top) or 50 μM MG132 + 200 mM CHX (bottom). Band intensities were quantified relative to the protein amount at 0 h and are indicated underneath the blot. α-TUBULIN was used as a loading control. Three independent experiments were performed with similar results. WT, wild type.

(E) In vivo degradation of RHD3. CHX (200 mM), 50 μM MG132, and 0.5 μM ConcA were used to treat 7-d-old seedlings for 24 h. The band intensities were quantified relative to the protein amount without CHX and are listed underneath the blot. Two independent experiments were performed with similar results.

RHD3) plants was reduced compared to that in *rhd3-8* (*RHD3pro*:*YFP-RHD3*) plants (Figure 8A).

On the other hand, when we transiently coexpressed YFP-RHD3 with or without LNP1 and LNP2 in *N. benthamiana* leaves, purified YFP-RHD3 was highly ubiquitinated in the presence of LNP1 and LNP2 (Figure 8B). Mammalian mLnp1 purified from mammalian cells has a ubiquitin ligase activity; yet, its substrate(s) has not been reported (Zhao et al., 2016). We then used an *Escherichia coli*–based plant ubiquitination cascade system (Han et al., 2017) to investigate whether Arabidopsis LNP1 and LNP2 have a ubiquitin ligase activity. As indicated in Figure 8C, when LNP1-mCherry was coexpressed with ubiquitin, E1, and E2 together, it did possess a ubiquitin ligase activity (Figure 8C). Similarly, LNP2 also possessed a ubiquitin ligase activity (Figure 8D).

mLnp1 is believed to have no typical HECT domain or RING finger (Zhao et al., 2016). To understand how LNPs may execute a ubiquitin ligase activity, we modeled the structure of the N and C termini of LNPs from Arabidopsis, yeast, and mammalian cells based on trRosetta (Yang et al., 2020), a non-homolog-based de novo protein prediction algorithm. It appeared that the N terminus of LNPs formed a helix and the C terminus started with a helix(es) following by a RING-like zinc finger structure (Supplemental Figure 9A). This structure resembles that of the C-terminal half of

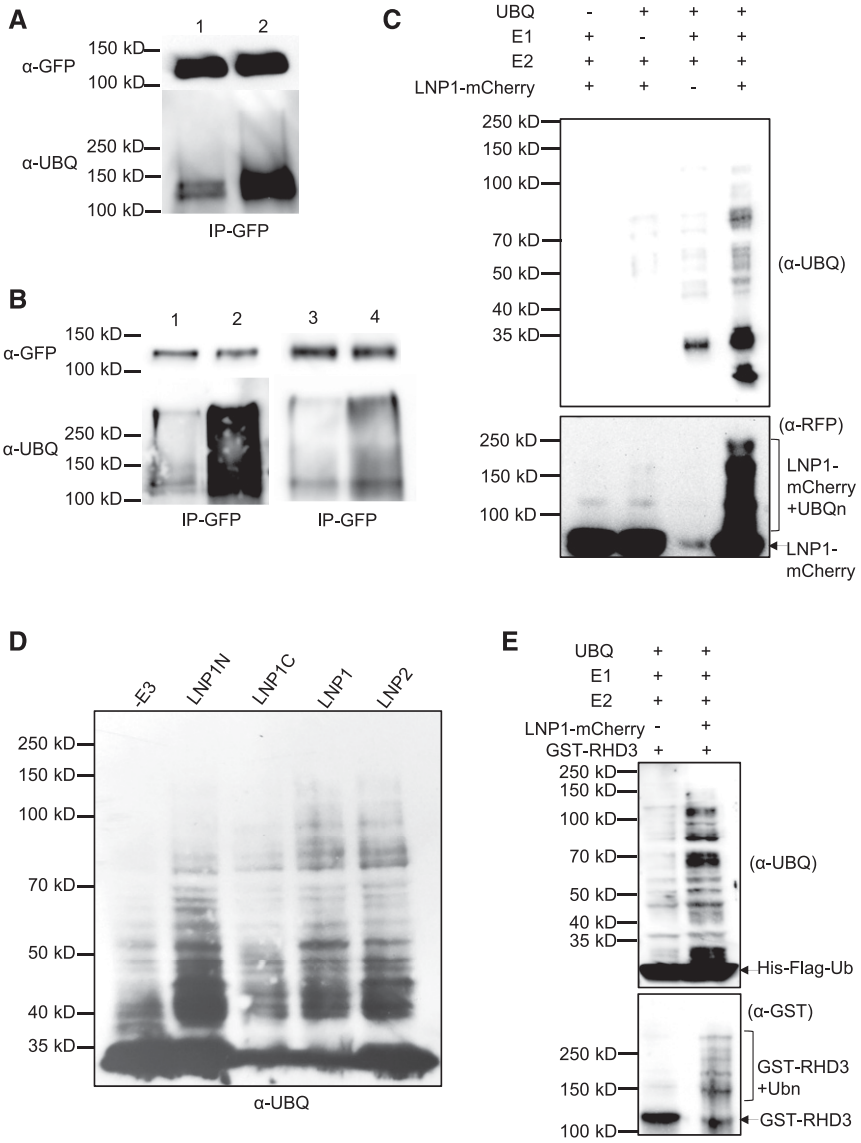

Figure 8. LNP Proteins Are Required for Ubiquitination of RHD3.

(A) RHD3 is less ubiquitinated in *lnp1-1 lnp2-1* mutant plants. Using GFP-trap beads, YFP-RHD3 was extracted and purified from *rhd3-8 lnp1-1 lnp2-1* (*RHD3*$_{pro}$:*YFP-RHD3*; lane 1) or *rhd3-8* (*RHD3*$_{pro}$:*YFP-RHD3*; lane 2) plants. Five independent experiments were performed with similar results. IP, immunoprecipitation; UBQ, ubiquitin.

(B) RHD3 is highly ubiquitinated in the presence of LNP1 and LNP2. YFP-RHD3 and HA-UB were coexpressed with LNP1-RFP (lane 2) and LNP2-RFP (lane 4) or without LNP1-RFP (lane 1) and LNP2-RFP (lane 3) in *N. benthamiana* leaves. Forty-eight hours after infiltration, YFP-RHD3 was purified with GFP-trap beads. Three independent experiments were performed with similar results. IP, immunoprecipitation; UBQ, ubiquitin.

(C) LNP1 has E3 ubiquitin ligase activity in the *E. coli*–based reconstituted bacterial system. The *E. coli* BL21 (DE3) strains expressing Arabidopsis (At-) UBA1-S (E1), At-UBC8-S (E2), His-Flag-UBQ10 (UBQ), and LNP1-mCherry, or strains missing one of these components as indicated, were analyzed by immunoblot using anti-UBQ or anti-RFP antibodies.

(D) LNP2, the N terminus, and C terminus of LNP1 have E3 ubiquitin ligase activity in the *E. coli*–based reconstituted bacterial system. The *E. coli* BL21 (DE3) strains expressing At-UBA1-S (E1), At-UBC8-S (E2), His-Flag-UBQ10 without E3 (-E3), or with LNP1N-mCherry, LNP1C-mCherry, LNP1-mCherry, or LNP2-mCherry.

(E) Ubiquitination of RHD3 by LNP1 in the *E. coli*–based the reconstituted bacterial system. GST-RHD3 was expressed together with other ubiquitination components in the presence (right lane) or absence (left lane) of LNP1-mCherry. Ub, ubiquitin; Ubn, ubiquitins; UBQ, ubiquitin.

gp78, which contains a helical G2BR that binds to its cognate E2, a helical CUE domain that can bind ubiquitin, and a RING finger domain (Supplemental Figure 9B; Das et al., 2009, 2013). gp78 is an E3 ligase regulates ER-associated degradation by ubiquitination (Fang et al., 2001). When the N and C termini of Arabidopsis LNP1 were tested, we revealed that both termini possessed a ubiquitin ligase activity (Figure 8D). We then asked whether LNP1 can directly mediate the ubiquitination of RHD3. When glutathione S-transferase (GST)-RHD3 was coexpressed with LNP1-mCherry in this system, polyubiquitinated GST-RHD3 were observed (Figure 8E). These results indicated that Arabidopsis LNP1 is a functional E3 ubiquitin ligase that can directly mediate the ubiquitination of RHD3.

DISCUSSION

We have identified two plant LNP homologs, LNP1 and LNP2, and show that Arabidopsis *lnp1-1 lnp2-1* mutant cells exhibit sheet-like ER with dense tubules. This indicates that Arabidopsis LNPs are required for the maintenance of normal tubular ER morphology. Because neither single mutant *lnp1-1* nor *lnp2-1* has obvious defects in plant cell development, but the double mutant *lnp1-1 lnp2-1* shows significantly defective cell growth with sheet-like ER in the cells, this suggests functional redundancy between LNP1 and LNP2.

It has been shown that the dysregulation of the ER could lead to the altered targeting of secretory vesicles (Qi et al., 2016) as well as abnormal endosome streaming and endocytosis (Stefano et al., 2015). This could at least partially account for the defective cell development observed in *lnp1-1 lnp2-1* plants. It was suggested, based on the increased mesh size of the cortical tubular ER in developed cells of *lnp* mutants (Kriechbaumer et al., 2018; Ueda et al., 2018), that Arabidopsis LNPs are not involved in the formation of the tubular ER network but instead the cisternal ER network. Here, we found that in young developing cells of the *lnp1 lnp2* mutant, the cortical ER is more sheeted with dense junctions, while in developed cells the cortical ER has increased mesh size, as reported by Kriechbaumer et al. (2018) and Ueda et al. (2018). In both developing and developed cells, the cytoplasmic ER aggregates with dense ER tubules. We therefore believe that Arabidopsis LNPs are functional homologs of yeast and mammalian LNP that they are involved in the formation and maintenance of a tubular ER. Why, in *lnp1 lnp2* mutant plant cells, do dense ER tubules tend to clump in the cytoplasm? Perhaps significantly increased cortical ER clumps with dense junctions formed in *lnp1 lnp2* cannot be properly held in the cortical region due to the lack of physical anchoring points. In this regard, it is noted that in yeast quadruple *ist2 tcb1/2/3* mutant cells, the cortical ER is collapsed due to the lack of ER–plasma membrane (PM) contact sites as physical anchoring points (Manford et al., 2012).

How are Arabidopsis LNPs involved in the formation of a tubular ER? In this study, we found that Arabidopsis LNP1 and LNP2 directly interact with RHD3. Both Arabidopsis LNP1 and LNP2 are localized on some three-way junctions of the ER. Interestingly, their localization to three-way junctions of the ER is lost in *rhd3* mutants or in the presence of dominant-negative forms of RHD3. In addition, when transiently overexpressed in the *N. benthamiana* leaves alone, LNP1 and LNP2 are also observed on the ER tubules, but when coexpressed with RHD3, both are only localized on three-way junctions. Thus, it is likely that LNPs could be recuited by RHD3 to the 3-way junctions and act together with RHD3.

We found that, in the presence of LNP1, newly formed three-way junctions of the ER are stable, while in the absence of LNP1, newly formed three-way junctions of the ER are less stable. We conclude that LNP1 and LNP2, if they are recruited successfully to newly formed three-way junctions of the ER, can suppress the fusion action of RHD3. This suppression could prevent excessive fusion of ER tubules, thereby resulting in a stable three-way junction of the ER. This conclusion is based on the three following evidences: (1) LNPs can suppress the formation of dense tubular ER caused by overexpression of RHD3 in plant cells, (2) LNPs can suppress the fusion action of RHD3 in yeast cells, and (3) *lnp1-1 lnp2-1* plants have an ER with dense junctions in the cells phenocopying the overexpression of RHD3. Contrary to this observation, in a recent publication by Kriechbaumer et al. (2018), Arabidopsis LNPs were proposed to not play a role in stabilization of three-way junctions of the ER. However, the authors only analyzed the stability of three-way junctions as a whole, but not the stability of newly formed three-way junctions in transient overexpression of LNPs. Indeed, an analysis of the pre-existing junctions in mammalian cells also reveals no difference between mLnp1-positive and mLnp1-negative junctions (Chen et al., 2015). But by limiting the observation to nascent three-way junctions, a very dramatic difference was documented by Chen et al. (2015). Thus, it is likely that LNPs predominantly work on newly formed junctions.

How do Arabidopsis LNPs suppress the fusion action of RHD3? In this study, we found that the overexpression of RHD3 with either LNP1 or LNP2 resulted in a reduced accumulation of RHD3 compared to overexpression of RHD3 alone. On the other hand, in *lnp1-1 lnp2-1* plants, the level of RHD3 is higher than that in wild-type plants. Our semi–in vitro cell-free and in vivo protein degradation assays suggested that in the absence of LNP1 and LNP2, RHD3 is degraded more slowly. It is likely that Arabidopsis LNPs mediate the degradation of RHD3. How could this happen? We found that in *lnp1 lnp2* mutants, the ubiquitination level of RHD3 is reduced, while in the presence of LNP1 and LNP2, the ubiquitination level of RHD3 is increased. By using a reconstituted *E. coli*–based ubiquitin system (Han et al., 2017), we revealed that in Arabidopsis both LNP1 and LNP2 protein have a ubiquitin ligase activity and that LNP1 directly regulates the ubiquitination level of RHD3 in plants. Therefore, the degradation of RHD3 promoted by LNPs is through a ubiquitination-based protein degradation pathway that involves LNPs acting as E3 ligases.

mLNP1 is said to not contain any typical E3 ligase domains known (Zhao et al., 2016); yet, it possesses an E3 ligase activity. As an evolutionarily conserved family of proteins, it is interesting to note that, based on our protein structure modeling, the N and C termini of LNPs appeared to have a structure resembling the cytosolic C-terminal half of gp78. The cytosolic C terminus of gp78 has a helical G2BR domain that binds to its cognate E2, a helical CUE domain that binds ubiquitin, and a RING finger domain that serves as a scaffold that brings E2 and the substrate together (Das et al., 2009, 2013). It has been shown that the N terminus of mammalian Lnp1 possesses a ubiquitin ligase activity (Zhao et al., 2016), Here, we found that both the N and C termini of Arabidopsis

LNP1 had a ubiquitin ligase activity. LNPs may be analogous to gp78 such that the N-terminus of LNP1 may act as G2BR domain of gp78 binds to E2, the coiled-coil domain may act as CUE domain of gp78 binds ubiquitin, and the zinc finger domain may serve as a RING domain to enhance the ubiquitination. It will be interesting to conduct site-directed mutagenesis analyses to understand the functional mode of LNPs. Although the level of RHD3 is elevated in *lnp1-1 lnp2-1* mutant plants, the level of other ER-localized proteins is not. We thus think that Arabidopsis LNPs do not broadly promote the degradation of ER proteins. Finally, in our in vivo protein degradation assay, the degradation of RHD3 was almost fully blocked in the absence of LNP1 and LNP2 as well as in the presence of both MG132 and ConcA, but MG132 or ConcA alone did not fully inhibit it. This suggests that LNP-mediated ubiquitination of RHD3 can lead to a 26S proteasome–based RHD3 degradation as well as a selective autophagy-based protein degradation.

Based on what we found here, we propose a model for how LNPs work together with RHD3 to regulate the formation of a tubular ER network. RHD3 molecules localized on two different ER membranes tether different ER tubules together by a dimerization (Sun and Zheng, 2018). After a GTP hydrolysis–dependent conformational change, RHD3 molecules will pull and fuse tethered ER membranes together to form a junction, after which LNPs may be recruited to three-way junctions through interaction with RHD3. Next, RHD3 on a newly formed junction will be removed by LNP-dependent protein degradation to avoid excessive fusion. In this way, the nascent junction will be stabilized without supernumerary RHD3 molecules on the junctions. In *lnp1-1 lnp2-1* mutant or overexpression of RHD3, due to the paucity of LNPs, excessive RHD3 molecules accumulate on the junctions, whose fusion activity will cause unnecessary membrane fusion, resulting in a dense tubular ER network in the cell.

METHODS

Molecular Cloning

The 3-in-1 BiFC vector was modified based on the pDOE04 vector (Gookin and Assmann, 2014). The original P19 fragment was replaced by the mCherry-HDEL sequence within *Kpn*I-*Nru*I cutting sites. RHD3, LNP1, LNP2, Sey1p, CER6, and p24 for BiFC systems were cloned into the 3-in-1 vector through the AQUA cloning method (Beyer et al., 2015). To generate LNP1-NubG and LNP2-NubG, LNP1 and LNP2 were first cloned with primers LNP1-FP/RP and LNP2-FP/RP into the pCR8/GW/TOPO entry vector (Invitrogen). Next, these two entry vectors were used to perform gateway reactions with pNX22-DEST. To generate *35Spro:LNP1-YFP* and *35Spro:LNP2-YFP*, the two entry vectors were used to perform gateway reactions with pEarleyGate 101. To generate *LNP1pro:LNP1-YFP* and *LNP2pro:LNP2-YFP*, the promoters of LNP1 and LNP2 were amplified with primers LNP1pro-FP/RP and LNP2pro-FP/RP from Arabidopsis genomic DNAs and cloned into pCambia1300 together with LNP1-YFP or LNP2-YFP, which was amplified from *35Spro:LNP1-YFP* and *35Spro:LNP2-YFP*. To create LNP1-RFP or LNP2-RFP, LNP1 or LNP2 was fused with red fluorescent protein (RFP) and cloned into pCambia1300 with *Xba*I-*Bam*HI sites. To create mCherry-HDEL or RFP-HDEL, the ER signal peptide and the HDEL sequence were added to the N and C termini of RFP or mCherry with PCR and then cloned into pCambia1300. To generate mCherry-RHD3, the GFP fragment of pVKH18-GFP-RHD3 (Chen et al., 2011) was replaced by mCherry with *Xba*I and *Sal*I sites. For the constructs of yeast ER fusion assay, the RHD3 vector was created as previously described by Sun and Zheng (2018). To express Arabidopsis (*Arabidopsis thaliana*) LNP1 and LNP2 in yeast cells, the yeast endogenous Lnp1p promoter was cloned into p413PGD vector (HIS3) and followed by LNP1 or LNP2 gene sequences. All primers used are listed in Supplemental Table 1.

Plant Materials and Growth Conditions

All the seeds of the mutants, including *lnp1-1* (GK607D07), *lnp1-2* (SK2564), *lnp2-1* (SALK_028863), *lnp2-2* (SALK_100743), and *rhd3-8* (SALK_025215), were ordered from the Arabidopsis Biological Resource Center. PCR and RT-PCR were used to identify homozygous lines. All primers used are listed in Supplemental Table 1.

The mutants *lnp1-1* (*LNP1pro:LNP1-YFP*), *lnp2-1* (*LNP2pro:LNP2-YFP*), *lnp1-1 lnp2-1* (*LNP1pro:LNP1-YFP*), and *lnp1-1 lnp2-1* (*LNP2pro:LNP2-YFP*) were generated by transforming *LNP1pro:LNP1-YFP* and *LNP2pro:LNP2-YFP* into *lnp1-1*, *lnp2-1*, or *lnp1-1 lnp2-1* mutants correspondingly. RFP-HDEL, mCherry-HDEL, and mCherry-RHD3 expressed *lnp1-1* (*LNP1pro:LNP1-YFP*) and *lnp2-1* (*LNP2pro:LNP2-YFP*) plants were generated by transforming the corresponding constructs into the mutant lines. *rhd3-8* (*LNP1pro:LNP1-YFP*), *rhd3-8* (*LNP2pro:LNP2-YFP*), plants were made by crossing *rhd3-8* with *lnp1-1* (*LNP1pro:LNP1-YFP*), *lnp2-1* (*LNP2pro:LNP2-YFP*). Col-0 (*35Spro:YFP-HDEL*) and *lnp1-1 lnp2-1* (*35Spro:YFP-HDEL*) were made by transforming YFP-HDEL into Col-0 wild-type and *lnp1-1 lnp2-1* plants. *rhd3-8 lnp1-1 lnp2-1* (*RHD3pro:YFP-RHD3*) plants were generated by crossing *lnp1-1 lnp2-1* with *rhd3-8* (*RHD3pro:YFP-RHD3*) plants (Sun and Zheng, 2018). All mutants and transgenic lines made in this study are listed in Supplemental Table 2.

Seedlings were grown on Arabidopsis medium (Haughn and Somerville, 1986) with 1% (w/v) Suc at 22 to 24°C under continuous light (80 to 100 μE m^{-1} s^{-1} photosynthetically active radiation).

Transient Expression in *Nicotiana benthamiana* and *Nicotiana tabacum* Leaves

N. benthamiana or *N. tabacum* plants with three or four leaves were used for infiltration. Agrobacterium carrying different constructs was grown in Luria-Bertani liquid medium at 28°C overnight. Next, the agrobacteria were resuspended in infiltration buffer (100 μM acetosyringone and 10 mM $MgCl_2$). The final $OD_{600\ nm}$ was 0.01 or 0.1. Images were taken or proteins were extracted 2 d after infiltration.

Confocal Microscopy

The most images were observed with a Leica SP8 point-scanning confocal system on a Leica DMI6000B inverted microscope equipped with spectral fluorescent light detectors (three photomultiplier tubes, one hybrid high-sensitivity detector). A 63×/1.4 oil objective was used for all the imaging. A 488 nm laser was used to excite YFP, and a 552 nm laser was used to excite RFP/mCherry. Two channels were excited sequentially. Emission filters were set as 490 to 560 nm for YFP and as 580 to 660 nm for RFP/mCherry. For quantification of the number of cells with the sheet ER, cells have more than 50% of area covered by sheet-like ER were defined as cells with sheet ER. An ER is defined as ER sheet when its area occupies several three-way junctions. At least 50 cells were examined in each condition. Data are from three different repeats; ***P value < 0.001 (*t* test; Supplemental File 1).

For observing the stability of three-way junctions, a quorum WaveFX-X1 spinning disk confocal system and a 63×/1.4 numerical aperture oil lens was used. A 491 nm laser was used to excite YFP and a 568 nm laser was used to excite RFP/mCherry. Time-lapse images were taken every second.

Airyscan Superresolution Microscopy

A Zeiss LSM 880 microscope with an Airyscan module was used for superresolution microscopy imaging. Three-day-old seedlings were picked and mounted in the water for imaging, under a 63× oil immersion objective. YFP and mCherry were excited at 514 and 561 nm, respectively. Resolution versus sensitivity Airyscan mode was used for imaging. Airyscan processing was performed with ZEN imaging software. For post-image editing, Fiji (Fiji is just ImageJ) was used (Schindelin et al., 2012).

Mating-Based SUS

The SUS is a method to study the protein–protein interactions between integral membrane proteins. In this system, two integral membrane proteins to be studied are fused to two different ubiquitin moieties: a C-terminal ubiquitin moiety (Cub, residues 35 to 76) and a mutated N-terminal ubiquitin moiety (NubG, residues 1 to 34; Obrdlik et al., 2004). The Cub-tagged RHD3 and NubG-tagged proteins were transformed into haploid yeast strains THY.AP4 and THY.AP5, respectively (Obrdlik et al., 2004). After transformation, colonies were picked and inoculated in Synthetic Complete (SC) selection liquid medium (-Leu for AP4 and -Trp for AP5) overnight at 28°C. The AP4 (Cub) and AP5 (NubG) suspensions were mixed and plated on YPD plates for mating. After 6 to 8 h at 28°C, mated cells were streaked onto -Leu-Trp (-LT) selection plates and incubated at 28°C for 2 d. Diploid cells were collected, inoculated in -LT liquid medium, and incubated at 28°C overnight. Next, the cells were resuspended in water and the $OD_{600\ nm}$ values were measured. Suspensions were diluted into OD = 1, 0.1, and 0.01. Next, 15 μL per spot was dropped on -LT plates for mating control or on -Leu-Trp-His plates for interaction test. Plates were incubated at 28°C for 2 d.

ER Fusion Assay in Yeast Cells

Different constructs were transformed into two different *Δsey1p* mutant haploid cells: ACY53 (ss-RFP-HDEL) and ACY54 (free GFP; Anwar et al., 2012). Cells were grown to an $OD_{600\ nm}$ of 0.1 to 0.4, mixed, and concentrated in YPD medium. A 5-μL cell suspension was dropped on a 1-mm-thick SC medium pad and grown at 30°C for 40 to 60 min. Images were taken at 20-s intervals.

Coimmunoprecipitation

Plant tissues (infiltrated *N. benthamiana* leaves or seedlings) were ground to a powder in liquid nitrogen and extracted with extraction buffer (50 mM Tris-HCl, pH 7.5, 150 mM NaCl, 10% [v/v] glycerol, 0.5% [v/v] IGEPAL CA-630 [catalog no. I8896; Sigma-Aldrich], and 1% [v/v] of Protease Inhibitor Cocktail [catalog no. P9599; Sigma-Aldrich]). For purification of ubiquitinated YFP-RHD3, 50 μM MG132 and 10 mM N-ethylmaleimide were added in the extraction buffer. The solution was homogenized to an even mixture and centrifuged at 17,000*g* for 10 min at 4°C. Next, the supernatant was collected, and 25 μL of GFP-Trap_MA beads (catalog no. gtma-20; Chromotek) was washed three times with wash buffer (10 mM Tris-HCl, pH 7.5, and 150 mM NaCl). The protein lysate was added to the washed beads and incubated for 1 h at 4°C. The beads were magnetically separated and washed three times with wash buffer. Next, the beads were resuspended in 50 μL of 2× SDS-loading buffer and boiled for 10 min. The solution was centrifuged, and the supernatant was used for protein gel blot.

Semi–In Vitro Cell-Free Protein Degradation Assay

Semi–in vitro cell-free protein degradation assays were performed as previously described by Wang et al. (2009). Total protein was extracted using degradation buffer (50 mM Tris-HCl, pH 7.5, 150 mM NaCl, 0.5% [v/v] Nonidet P-40, 10 mM $MgCl_2$, and 10 mM ATP) with or without 50 μM MG132. After the centrifugation, the supernatant was taken and incubated at room temperature. At each indicated time points, 50 μL of extract was taken to mix with 2× SDS-loading buffer and boiled to stop the reaction before immunoblotting.

In Vivo Protein Degradation Assay

For in vivo protein degradation assay, 7-d-old seedlings were treated with 200 μM CHX, 50 μM MG132, and 0.5 μM ConcA as indicated. At different time points, seedlings were collected and total proteins were extracted with 2× SDS-loading buffer and used in protein gel blot to detect the degradation rate of RHD3.

In Vitro Protein Ubiquitination Assay in *Escherichia coli*

Two modified Duet expression vectors, pCDFDuet and pACYCDuet (Novagen), were used for in vitro ubiquitination assay. Transmembrane domain–deleted LNP1, LNP2, and the N and C termini of LNP1 fused with mCherry at their C termini were cloned together with UBC8-S into the pACYCDuet vector. Transmembrane domain–deleted RHD3 fused with GST at its N terminus was cloned together with AtUBA1-S into the pCDFDuet vector. These two plasmids, together with the pET-28a vector containing His-Flag-UBQ10, were cotransformed into *E. coli* BL21 (DE3) competent cells. BL21 (DE3) cells were cultured in 3 mL of Luria-Bertani liquid medium with corresponding antibiotics at 37°C. The expression of recombinant proteins was induced by isopropyl β-D-1-thiogalactopyranoside when OD reached 0.4 to 0.6. After the induction, the bacteria were further grown at 28°C for 12 h. Next, total crude proteins were extracted with 2× SDS-loading buffer and were separated by SDS-PAGE and analyzed by immunoblot.

Immunoblotting

Protein samples were boiled for 5 min. After a 2-min centrifugation at 13,000 rpm, the supernatants were loaded on a 10% SDS-PAGE gel. Rabbit anti-RHD3CT antibody (PHY0765S; PhytoAB; 1:10,000 dilution), anti-AGB1 antibody (PHY0956S; PhytoAB; 1:1000 dilution), anti-LPAT2 antibody (PHY0873S; PhytoAB; 1:1000 dilution), anti-actin antibody (AS13 2640; Agrisera; 1:4000 dilution), anti-GST antibody (AS17 4147; Agrisera; 1:2000 dilution), and anti-ubiquitin antibody (AS08 307A; Agrisera; 1:1000 dilution) were used for the protein gel blot. Mouse anti-tubulin (T6074; Sigma-Aldrich; 1:4000) and goat anti-mouse (A4914-1ML; Sigma-Aldrich; 1:10,000) were used as the loading control of the protein gel blot. For the blotting after immunoprecipitation, a rabbit anti-GFP antibody (ab32146; Abcam) at 1:5000 dilution or a rabbit anti-RFP (ab34771; Abcam) at 1:2000 dilution was used. The secondary anti-rabbit IgG-peroxidase (Sigma-Aldrich) was used at 1:5000 dilution. The intensity of bands was quantified relatively to the reference band by ImageJ.

Transmission Electron Microscopy

Small pieces (1.5 mm × 2 mm) of the wild-type and *lnp1-1 lnp2-1* double mutant cotyledons were cut and fixed in 2.5% (w/v) glutaraldehyde in 0.1 M sodium cacodylate buffer, pH 7.4, for 24 h at 4°C. After rinsing three times for 10 min each in washing buffer at room temperature, the samples were postfixed, embedded, and thin sectioned as described by Movahed et al. (2019). The sectioned samples were examined in a Tecnai T12 transmission electron microscope (FEI) operating at 120 kV. Images were recorded using an AMT XR80C charge-coupled-device camera system (FEI).

Phylogenetic Analysis and Protein Structure Modeling

The phylogenetic tree was generated by PhyloGenes (http://www.phylogenes.org/) based on LNP1 (AT2G24330) with the default settings. The homologs of LNP1 from 17 different species, including human, mouse (*Mus musculus*), rat (*Rattus norvegicus*), zebrafish (*Danio rerio*), nematode (*Caenorhabditis elegans*), fruitfly (*Drosophila melanogaster*), budding yeast (*Saccharomyces cerevisiae*), fission yeast (*Schizosaccharomyces pombe*), slime mold (*Dictyostelium discoideum*), sorghum (Sorghum bicolor), maize (*Zea mays*), rice (*Oryza sativa*), *N. tabacum*, Chinese cabbage (*Brassica rapa* subsp. *pekinensis*), Arabidopsis, cotton (Gossypium hirsutum), and *Physcomitrella patens*, were chosen. The structures of the N and C termini of LNPs from Arabidopsis, yeast, and mammalian cells were predicted by trRosetta (Yang et al., 2020), a non-homolog-based de novo protein prediction algorithm. A text file of the alignment used is provided in Supplemental File 2.

Accession Numbers

Sequence data from this article can be found in the Arabidopsis Genome Initiative database under the following accession numbers: *RHD3* (AT3G13870), *LNP1* (AT2G24330), *LNP2* (AT4G31080), *EF1αA4* (AT5G60390), *AGB1* (AT4G34460), *LPAT2* (AT3G57650), ACTIN 2 (AT3G18780), and α-*TUBULIN* (AT4G14960).

Supplemental Data

Supplemental Figure 1. 3-in-1 BiFC system and primary structure and sequence of LNP proteins.

Supplemental Figure 2. Phylogenetic analysis of LNPs found in eukaryotes.

Supplemental Figure 3. RHD3 physically interacts with LNP1 and LNP2.

Supplemental Figure 4. The localization of LNPs is dependent on RHD3.

Supplemental Figure 5. Overexpression of RHD3 generates ER sheets with dense ER junctions.

Supplemental Figure 6. Sey1p does not interact with LNP1 and LNP2 in *N. benthamiana* cells.

Supplemental Figure 7. LNPs promote degradation of RHD3.

Supplemental Figure 8. LNP1 promotes the degradation of RHD3 in vivo.

Supplemental Figure 9. Modeling of mLnp1, scLnp1 and AtLNP1 and the structure of gp78.

Supplemental Table 1. List of primers used for cloning, genotyping and RT-PCR-based gene expression.

Supplemental Table 2. List of mutants and transgenic lines generated and used in this study.

Supplemental File 1. Statistical results tables.

Supplemental File 2. Alignment used for the phylogenetic analysis in Supplemental Figure 2.

Supplemental Movie 1. The dynamic of a newly formed 3-way junction without LNP1-RFP.

Supplemental Movie 2. The Dynamic of a newly formed 3-way junction with LNP1-RFP.

Supplemental Movie 3. ER fusion in *Δsey1p* yeast cells.

Supplemental Movie 4. ER fusion in *Δsey1p* yeast cells expressing RHD3.

Supplemental Movie 5. ER fusion in *Δsey1p* yeast cells expressing Sey1p.

Supplemental Movie 6. ER fusion in *Δsey1p* yeast cells expressing RHD3 and LNP1.

Supplemental Movie 7. ER fusion in *Δsey1p* yeast cells expressing RHD3 and LNP2.

Supplemental Movie 8. ER fusion in *Δsey1p* yeast cells expressing Sey1p and LNP1.

Supplemental Movie 9. ER fusion in *Δsey1p* yeast cells expressing Sey1p and LNP2.

ACKNOWLEDGMENTS

We thank the Cell Imaging and Analysis Network and the Advanced BioImaging Facility at McGill University for confocal microscopy imaging support; the Neuro Microscopy Imaging Centre, McGill University, for Airyscan microscopy imaging support; and Dongping Lu (Institute of Genetics and Developmental Biology, Chinese Academy of Sciences, Hebei, China) for providing the bacteria-based reconstituted plant ubiquitination cascade. This research was supported by the Natural Sciences and Engineering Research Council of Canada (discovery grant 315863 and Discovery Accelerator Supplement award to H.Z.) and by the Chinese Scholarship Council (scholarship to J.S.).

AUTHOR CONTRIBUTIONS

J.S. designed and performed the experiments and wrote the article; N.M. performed the transmission electron microscopy experiments; and H.Z. designed and conceived the experiments and wrote the article.

Received December 17, 2019; revised May 27, 2020; accepted June 30, 2020; published July 2, 2020.

REFERENCES

Angelos, E., Ruberti, C., Kim, S.J., and Brandizzi, F. (2017). Maintaining the factory: The roles of the unfolded protein response in cellular homeostasis in plants. Plant J. **90:** 671–682.

Anwar, K., Klemm, R.W., Condon, A., Severin, K.N., Zhang, M., Ghirlando, R., Hu, J., Rapoport, T.A., and Prinz, W.A. (2012). The dynamin-like GTPase Sey1p mediates homotypic ER fusion in *S. cerevisiae*. J. Cell Biol. **197:** 209–217.

Beyer, H.M., Gonschorek, P., Samodelov, S.L., Meier, M., Weber, W., and Zurbriggen, M.D. (2015). AQUA cloning: A versatile and simple enzyme-free cloning approach. PLoS One **10:** e0137652.

Chen, J., Qi, X., and Zheng, H. (2012a). Subclass-specific localization and trafficking of Arabidopsis p24 proteins in the ER-Golgi interface. Traffic **13:** 400–415.

Chen, J., Stefano, G., Brandizzi, F., and Zheng, H. (2011). Arabidopsis RHD3 mediates the generation of the tubular ER network and is required for Golgi distribution and motility in plant cells. J. Cell Sci. **124:** 2241–2252.

Chen, S., Cui, Y., Parashar, S., Novick, P.J., and Ferro-Novick, S. (2018). ER-phagy requires Lnp1, a protein that stabilizes

rearrangements of the ER network. Proc. Natl. Acad. Sci. USA **115:** E6237–E6244.

Chen, S., Desai, T., McNew, J.A., Gerard, P., Novick, P.J., and Ferro-Novick, S. (2015). Lunapark stabilizes nascent three-way junctions in the endoplasmic reticulum. Proc. Natl. Acad. Sci. USA **112:** 418–423.

Chen, S., Novick, P., and Ferro-Novick, S. (2012b). ER network formation requires a balance of the dynamin-like GTPase Sey1p and the Lunapark family member Lnp1p. Nat. Cell Biol. **14:** 707–716.

Das, R., Liang, Y.H., Mariano, J., Li, J., Huang, T., King, A., Tarasov, S.G., Weissman, A.M., Ji, X., and Byrd, R.A. (2013). Allosteric regulation of E2:E3 interactions promote a processive ubiquitination machine. EMBO J. **32:** 2504–2516.

Das, R., Mariano, J., Tsai, Y.C., Kalathur, R.C., Kostova, Z., Li, J., Tarasov, S.G., McFeeters, R.L., Altieri, A.S., Ji, X., Byrd, R.A., and Weissman, A.M. (2009). Allosteric activation of E2-RING finger-mediated ubiquitylation by a structurally defined specific E2-binding region of gp78. Mol. Cell **34:** 674–685.

English, A.R., and Voeltz, G.K. (2013). Endoplasmic reticulum structure and interconnections with other organelles. Cold Spring Harb. Perspect. Biol. **5:** a013227.

Fang, S., Ferrone, M., Yang, C., Jensen, J.P., Tiwari, S., and Weissman, A.M. (2001). The tumor autocrine motility factor receptor, gp78, is a ubiquitin protein ligase implicated in degradation from the endoplasmic reticulum. Proc. Natl. Acad. Sci. USA **98:** 14422–14427.

Gookin, T.E., and Assmann, S.M. (2014). Significant reduction of BiFC non-specific assembly facilitates in planta assessment of heterotrimeric G-protein interactors. Plant J. **80:** 553–567.

Grefen, C., Lalonde, S., and Obrdlik, P. (2007). Split-ubiquitin system for identifying protein-protein interactions in membrane and full-length proteins. Curr. Protoc. Neurosci. **5:** 5 27.

Han, Y., Sun, J., Yang, J., Tan, Z., Luo, J., and Lu, D. (2017). Reconstitution of the plant ubiquitination cascade in bacteria using a synthetic biology approach. Plant J. **91:** 766–776.

Haughn, G.W., and Somerville, C. (1986). Sulfonylurea-resistant mutants of *Arabidopsis thaliana*. Mol. Gen. Genet. **204:** 430–434.

Hooker, T.S., Millar, A.A., and Kunst, L. (2002). Significance of the expression of the CER6 condensing enzyme for cuticular wax production in Arabidopsis. Plant Physiol. **129:** 1568–1580.

Hu, J., Shibata, Y., Zhu, P.P., Voss, C., Rismanchi, N., Prinz, W.A., Rapoport, T.A., and Blackstone, C. (2009). A class of dynamin-like GTPases involved in the generation of the tubular ER network. Cell **138:** 549–561.

Kim, H.U., Li, Y., and Huang, A.H. (2005). Ubiquitous and endoplasmic reticulum-located lysophosphatidyl acyltransferase, LPAT2, is essential for female but not male gametophyte development in Arabidopsis. Plant Cell **17:** 1073–1089.

Kriechbaumer, V., Breeze, E., Pain, C., Tolmie, F., Frigerio, L., and Hawes, C. (2018). Arabidopsis Lunapark proteins are involved in ER cisternae formation. New Phytol. **219:** 990–1004.

Liu, Y., Zhang, C., Wang, D., Su, W., Liu, L., Wang, M., and Li, J. (2015). EBS7 is a plant-specific component of a highly conserved endoplasmic reticulum-associated degradation system in Arabidopsis. Proc. Natl. Acad. Sci. USA **112:** 12205–12210.

Manford, A.G., Stefan, C.J., Yuan, H.L., Macgurn, J.A., and Emr, S.D. (2012). ER-to-plasma membrane tethering proteins regulate cell signaling and ER morphology. Dev. Cell **23:** 1129–1140.

Movahed, N., Sun, J., Vali, H., Laliberté, J.F., and Zheng, H. (2019). A host ER fusogen is recruited by *Turnip mosaic virus* for maturation of viral replication vesicles. Plant Physiol. **179:** 507–518.

Nixon-Abell, J., Obara, C.J., Weigel, A.V., Li, D., Legant, W.R., Xu, C.S., Pasolli, H.A., Harvey, K., Hess, H.F., Betzig, E., Blackstone, C., and Lippincott-Schwartz, J. (2016). Increased spatiotemporal resolution reveals highly dynamic dense tubular matrices in the peripheral ER. Science **354:** aaf3928.

Obrdlik, P., et al. (2004). K+ channel interactions detected by a genetic system optimized for systematic studies of membrane protein interactions. Proc. Natl. Acad. Sci. USA **101:** 12242–12247.

Orso, G., Pendin, D., Liu, S., Tosetto, J., Moss, T.J., Faust, J.E., Micaroni, M., Egorova, A., Martinuzzi, A., McNew, J.A., and Daga, A. (2009). Homotypic fusion of ER membranes requires the dynamin-like GTPase atlastin. Nature **460:** 978–983.

Qi, X., Sun, J., and Zheng, H. (2016). A GTPase-dependent fine ER is required for localized secretion in polarized growth of root hairs1. Plant Physiol. **171:** 1996–2007.

Schindelin, J., et al. (2012). Fiji: An open-source platform for biological-image analysis. Nat. Methods **9:** 676–682.

Sparkes, I., Hawes, C., and Frigerio, L. (2011). FrontiERs: Movers and shapers of the higher plant cortical endoplasmic reticulum. Curr. Opin. Plant Biol. **14:** 658–665.

Sparkes, I.A., Runions, J., Kearns, A., and Hawes, C. (2006). Rapid, transient expression of fluorescent fusion proteins in tobacco plants and generation of stably transformed plants. Nat. Protoc. **1:** 2019–2025.

Stefano, G., Renna, L., Lai, Y., Slabaugh, E., Mannino, N., Buono, R.A., Otegui, M.S., and Brandizzi, F. (2015). ER network homeostasis is critical for plant endosome streaming and endocytosis. Cell Discov. **1:** 15033.

Sun, J., and Zheng, H. (2018). Efficient ER fusion requires a dimerization and a C-terminal tail mediated membrane anchoring of RHD3. Plant Physiol. **176:** 406–417.

Ueda, H., Ohta, N., Kimori, Y., Uchida, T., Shimada, T., Tamura, K., and Hara-Nishimura, I. (2018). Endoplasmic reticulum (ER) membrane proteins (LUNAPARKs) are required for proper configuration of the cortical ER network in plant cells. Plant Cell Physiol. **59:** 1931–1941.

Wang, F., Zhu, D., Huang, X., Li, S., Gong, Y., Yao, Q., Fu, X., Fan, L.M., and Deng, X.W. (2009). Biochemical insights on degradation of Arabidopsis DELLA proteins gained from a cell-free assay system. Plant Cell **21:** 2378–2390.

Wang, S., Narendra, S., and Fedoroff, N. (2007). Heterotrimeric G protein signaling in the Arabidopsis unfolded protein response. Proc. Natl. Acad. Sci. USA **104:** 3817–3822.

Wang, S., Tukachinsky, H., Romano, F.B., and Rapoport, T.A. (2016). Cooperation of the ER-shaping proteins atlastin, lunapark, and reticulons to generate a tubular membrane network. eLife **5:** e18605.

Westrate, L.M., Lee, J.E., Prinz, W.A., and Voeltz, G.K. (2015). Form follows function: The importance of endoplasmic reticulum shape. Annu. Rev. Biochem. **84:** 791–811.

Yang, J., Anishchenko, I., Park, H., Peng, Z., Ovchinnikov, S., and Baker, D. (2020). Improved protein structure prediction using predicted interresidue orientations. Proc. Natl. Acad. Sci. USA **117:** 1496–1503.

Yoshimoto, K., Hanaoka, H., Sato, S., Kato, T., Tabata, S., Noda, T., and Ohsumi, Y. (2004). Processing of ATG8s, ubiquitin-like proteins, and their deconjugation by ATG4s are essential for plant autophagy. Plant Cell **16:** 2967–2983.

Zhang, M., Wu, F., Shi, J., Zhu, Y., Zhu, Z., Gong, Q., and Hu, J. (2013). ROOT HAIR DEFECTIVE3 family of dynamin-like GTPases mediates homotypic endoplasmic reticulum fusion and is essential for Arabidopsis development. Plant Physiol. **163:** 713–720.

Zhao, Y., Zhang, T., Huo, H., Ye, Y., and Liu, Y. (2016). Lunapark is a component of a ubiquitin ligase complex localized to the endoplasmic reticulum three-way junctions. J. Biol. Chem. **291:** 18252–18262.

Zheng, H., and Chen, J. (2011). Emerging aspects of ER organization in root hair tip growth: lessons from RHD3 and atlastin. Plant Signal. Behav. **6:** 1710–1713.